



CHORUS

This is the accepted manuscript made available via CHORUS. The article has been published as:

Magnetless Circulators with Harmonic Rejection Based on N-Way Cyclic-Symmetric Time-Varying Networks

Ahmed Kord, Harish Krishnaswamy, and Andrea Alù

Phys. Rev. Applied **12**, 024046 — Published 22 August 2019

DOI: [10.1103/PhysRevApplied.12.024046](https://doi.org/10.1103/PhysRevApplied.12.024046)

Magnetless Circulators with Harmonic Rejection Based on N -Way Cyclic-Symmetric Time-Varying Networks

Ahmed Kord^{1,2}, Harish Krishnaswamy², and Andrea Alu^{1,3,4,5*}

¹*Department of Electrical and Computer Engineering, the University of Texas at Austin, Austin, TX 78712, USA*

²*Department of Electrical Engineering, Columbia University, New York, NY 10027, USA*

³*Photonics Initiative, Advanced Science Research Center, City University of New York, New York, NY 10031, USA*

⁴*Physics Program, Graduate Center, City University of New York, New York, NY 10026, USA*

⁵*Department of Electrical Engineering, City College of New York, New York, NY 10031, USA*

Abstract

Magnet-free circulators are crucial devices to enable full-duplex communications, with the goal of enhancing the spectral efficiency of wireless radios compared to currently deployed half-duplex systems. Nevertheless, implementations proposed to date at radio and millimeter-wave frequencies have been based on spatiotemporally modulating a *discrete number of non-linear* elements, such as varactors or switched capacitors which, despite achieving strong non-reciprocity, suffer from spurious emission in adjacent channels and limited power handling. These problems jeopardize the practical use of these components in many applications, including wireless communications and quantum computing, and make them less attractive compared to harmonic-free magnetic devices. In this paper, we address these problems by introducing N -way circulators, which consist of N spatiotemporally modulated angular-momentum (STM-AM) biased units connected either in series or in parallel, and modulated through a *rotating phase pattern*. We show that these circuits, for a sufficiently large N , effectively impart an overall linear and continuous angular-momentum bias, which significantly reduces spurious emission and increases the overall power handling. This, in turn, strengthens the argument of magnetless circulators compared to their magnetic counterparts, and opens exciting venues to address the realistic needs of practical systems.

I. INTRODUCTION

Time-reversal symmetry is a fundamental property in various physical and engineering domains, which implies that the laws governing such systems are invariant if the evolution of time is reversed. Breaking this symmetry is essential to realize non-reciprocal components such as isolators and circulators, which have many applications at different frequency bands of the electromagnetic spectrum. For instance, isolators are necessary in optical systems to protect laser sources from reflections. More importantly, circulators are crucial to enable full-duplex communications [1]-[7], which have been gaining a lot of interest recently in anticipation of future high-throughput applications that require simultaneous transmission and reception on the same frequency. Circulators also play a pivotal role in quantum computing for they allow the use of Josephson parametric amplifiers to amplify the extremely weak readout signals of quantum bits (qubits) without worrying about any potential instabilities or reflections that may alter the fragile quantum state [8]-[16]. Traditionally, non-reciprocity has been achieved through magnetic biasing of ferrite materials, leading to bulky and expensive devices that are incompatible with conventional integrated circuit (IC) technologies. In order to overcome these problems, a few magnetless implementations of non-reciprocal components have been pursued over the past few decades, based on self-biased hexaferrites and ferromagnetic nanowires [17]-[21], transistors [22]-[26], or parametrically modulated networks [27]-[52]. Among these different approaches, linear periodically time-varying (LPTV) circuits have shown the utmost promise to satisfy all the necessary requirements of practical systems. In this context, several new techniques have been proposed based on STM-AM biasing [27]- [35], N -path filtering [36], [37], and transmission line (TL) switching [38]-[42]. In particular, [27] showed that a cyclic-symmetric magnet-free circulator can be realized by coupling three resonators and modulating their oscillation frequencies with 120° phase-shifted periodic signals. Ref. [29] refined this concept and derived the necessary conditions to achieve optimal performance, which resulted in the first Watt-class magnetless circulator ever presented. Furthermore, [30] developed a differential STM-AM circulator that enhanced the performance in terms of several

metrics, particularly insertion loss and noise figure, which were reduced to 0.8 dB and 2.5 dB, respectively, the lowest among magnet-less circulators reported to date. Also, [31] presented a broadband circulator with a 20 dB isolation bandwidth of 140 MHz, and derived a theoretical bound on such critical metric. Moreover, [32] presented the first CMOS implementation of STM-AM circulators, thus reducing their size by orders of magnitude and permitting their low-cost and large-scale production. In parallel, these works have been accompanied by numerous advances using related concepts at different frequency ranges and in various physical domains [36]-[52]. In particular, Ref. [36] presented the first CMOS magnetless circulator based on staggered commutation of N -path filters to realize a highly miniaturized gyrator, which when embedded in a loop of reciprocal phase shifters yields the operation of a circulator. Ref. [38] has shown that the same gyrator can be built using switched TLs, which increases the bandwidth and reduces the modulation frequency compared to the N -path filter implementation by a factor of three. Ref. [39] relied on the same concept to develop the first Watt-class IC circulator, thus pushing this technology several steps forward. On the other hand, [40] presented an ultra-wideband circulator operating from 200 KHz to 200 MHz using sequentially switched co-axial cables. An IC implementation of the same concept was recently presented in [41] using a 0.2 μm Gallium Nitride (GaN) high electron mobility transistor (HEMT) technology.

Despite the significant improvements introduced in the above works, the maximum power handling of all magnetless circulators presented to date is still limited to a few Watts range. More importantly, they also suffer from intermodulation products (IMPs) that appear equally at all terminals for input excitation at any port. This issue not only poses an interference problem to adjacent channels, but it also effectively degrades the performance of the device itself. Specifically, these IMPs increase the insertion loss, because they draw power from the fundamental harmonic, and they also impose a restriction on the lowest possible modulation frequency to avoid aliasing from the image signals around the IMPs into the desired bandwidth around the fundamental frequency. Furthermore, they may perturb the fragile state of qubits in quantum systems or saturate

the sensitive frontend of a receiver in a wireless radio. These problems are all essentially due to the *discrete non-linear* nature of the synthesized effective bias, i.e., a discrete number of non-linear elements are modulated in time to break reciprocity, and the associated mixing issues. While these problems can be avoided by mechanically moving the device, instead of modulating it in time [47], such a solution is not practical at radio and mm-wave frequencies. Hence, a discrete number of modulated elements with a particular phase pattern that mimics the mechanical motion of the fluid is the only feasible solution for electronic circuits, as indeed was pursued by all previous works. But in this case, spurious emission seems non-avoidable due to frequency mixing between modulation and input signals. Ref. [30] proposed an initial solution to this problem based on connecting two single-ended (SE) circulators in a differential architecture. Assuming small input signals and ideal linear elements, differential STM-AM circulators can theoretically cancel all IMPs. In practice, however, non-linearities of the modulating elements, either based on solid-state varactors, switched capacitors, or superconducting quantum interference devices (SQUIDs), in addition to timing errors and device mismatches still result in large IMPs. Furthermore, these inevitable non-idealities impose a restriction on the maximum possible power handling due to compression of the modulating elements [29]. In this paper, we address these problem by generalizing the differential approach to N -way magnetless circulators, which consist of N differential units connected in series or in parallel and exhibiting a rotating phase pattern. We show that, for a sufficiently large N , the N -way circuits synthesize an effectively linear and continuous angular momentum bias that mimics a mechanical rotation, despite the fact that each constituent element imparts a discrete and non-linear bias. This is consistent with magnetized circulators, in which the aligned electron dipole moments imitate a continuous rotation at a macroscopic level, even though are in fact a collection of quantized spins. As a result, the N -way circuits significantly suppress the spurious emission at all their terminals for input excitation at any port and in the presence of all non-idealities. In other words, they *practically* become, from a terminal perspective,

linear time-invariant (LTI) systems even though the N constituent units are each non-linear and time-varying.

This paper is organized as follows. In Sec. II, we investigate the physical principles behind breaking reciprocity in cyclic-symmetric circulators and show how they are achieved in magnetic devices. In Sec. III, we develop four optimal single-ended STM-AM circulators that synthesize an effective angular momentum bias. In Sec. IV, we present the voltage- and current-mode differential architectures of all possible four topologies, and compare their performance to gain an insight into the pros and cons of each circuit. In Sec. V, we introduce the N -way STM-AM circulators and show that they straighten and linearize the overall effective angular-momentum bias, thus allowing to overcome the power handling and spurious emission limitations of all LPTV based implementations of magnetless circulators presented to-date. We validate these circuits by comparing the simulated results of a 1-way, a 2-way, a 4-way, and an 8-way circulator, using the voltage-mode bandstop/delta topology, which was experimentally validated in [30], as the unit element. Finally, we draw our conclusions and provide an outlook on future directions in Sec. VI.

II. EIGENMODES OF CYCLIC-SYMMETRIC CIRCULATION

By definition, the S -parameters of any cyclic-symmetric circulator can be written in the following form

$$\bar{\bar{S}}(\omega) = \begin{bmatrix} S_{11} & S_{31} & S_{21} \\ S_{21} & S_{11} & S_{31} \\ S_{31} & S_{21} & S_{11} \end{bmatrix}, \quad (1)$$

where $RL = -20 \log_{10}(|S_{11}|)$ is the circulator's return loss, $IL = -20 \log_{10}(|S_{21}|)$ is the insertion loss, and $IX = -20 \log_{10}(|S_{31}|)$ is the isolation. Notice that in the ideal case, $S_{11} = S_{31} = 0$ and $S_{21} = 1$, assuming transmission in the following order $1 \rightarrow 2 \rightarrow 3$. These parameters are in general frequency dispersive, calculated with respect to the port

impedance Z_0 , and optimized to maintain a certain level of insertion loss and isolation, typically 3 dB and 20 dB, respectively, over a finite bandwidth, which is centered around a particular design frequency, say f_0 . The eigenvalues of this matrix can be calculated using $\|\bar{S} - \lambda\bar{U}\| = 0$, where \bar{U} is the unitary matrix, which yields

$$\lambda_c = S_{11} + S_{21} + S_{31} \quad (2)$$

$$\lambda_+ = S_{11} + e^{-j2\pi/3} S_{21} + e^{+j2\pi/3} S_{31} \quad (3)$$

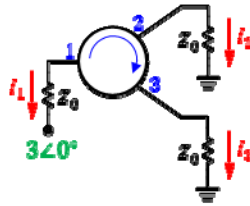
$$\lambda_- = S_{11} + e^{+j2\pi/3} S_{21} + e^{-j2\pi/3} S_{31}. \quad (4)$$

The eigenvectors associated with (2)-(4) are also given by

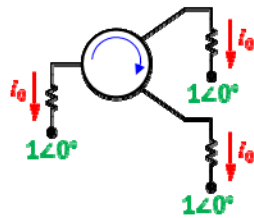
$$\bar{V}_0 = [1, 1, 1]^T \quad (5)$$

$$\bar{V}_+ = [1, e^{+j2\pi/3}, e^{-j2\pi/3}]^T \quad (6)$$

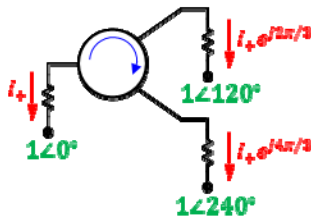
$$\bar{V}_- = [1, e^{-j2\pi/3}, e^{+j2\pi/3}]^T. \quad (7)$$



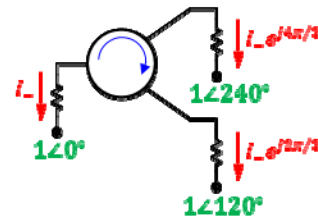
(a)



(b)



(c)



(d)

Figure 1: (a) Harmonic excitation at port 1 decomposed into a weighted summation of three components: (b) In-phase mode. (c) Clockwise mode. (d) Counter clockwise mode.

A harmonic excitation at any of the circulator's ports can be written as a summation of these eigenvectors. For instance, consider the excitation of port 1 as shown in Fig. 1(a) using a voltage source with an amplitude $3\angle 0^\circ$ and a matched source impedance Z_0 , at an arbitrary frequency f , while terminating the other two ports with matched loads. This circuit can be decomposed using superposition into three sub-circuits, as shown in Fig.

1(b)-(d) (notice that $\sum_{n=1}^3 e^{j(n-1)2\pi/3} = 0$). In Fig. 1(b), the applied voltage sources are identical in both magnitude and phase, which is mathematically represented by the eigenvector \bar{V}_0 . On the other hand, the voltage sources in Fig. 1(c) and Fig. 1(d) have the same magnitude but their phases increase by 120° either clockwise or counter-clockwise, which are also mathematically represented by the eigenvectors \bar{V}_+ and \bar{V}_- , respectively. Because of their distinctive phase pattern, we refer to these eigenvectors \bar{V}_0 , \bar{V}_+ , and \bar{V}_- as the in-phase (0), clockwise (+), and counter clockwise (-) modes, respectively. The generated currents at all ports can also be written as a weighted summation of these modes, i.e.,

$$I_n = I_0 + I_+ e^{+j(n-1)2\pi/3} + I_- e^{-j(n-1)2\pi/3}, \quad (8)$$

where n is the port index, and the unknown weights I_0 , I_+ , and I_- rely on the specific implementation of the circulator itself. If we assume that this implementation guarantees that: (i) the in-phase mode current I_0 is zero and (ii) the rotating modes I_\pm have the same amplitude but opposite phases, i.e., $I_\pm = I_g e^{\pm j\alpha}$, then (8) simplifies to

$$I_n = 2I_g \cos \left[(n-1) \frac{2\pi}{3} + \alpha \right]. \quad (9)$$

In the next sections, we explain how these two assumptions are satisfied in both magnetic and STM-AM circulators. Also, the phase α can be designed to be 30° at the center frequency f_0 , which when substituted in (9) results in $I_3 = 0$ and $I_1 = -I_2 = \sqrt{3}I_g$, thus isolating port 3 from excitations at port 1 and transmitting the input power exclusively to port 2. Similarly, impinging signals on port 2 or port 3 would be routed exclusively to port 3 and port 1, respectively. As the input frequency deviates from f_0 , however, α becomes different, thus reducing isolation and increasing insertion loss, which results in the typical dispersive S -parameters of circulators. It is worth mentioning that (9) neglects the impact of finite losses, which, if taken into account, will force the magnitudes of the rotating modes I_{\pm} , and consequently, the port currents $I_{1,2}$ to be slightly different, hence insertion loss becomes finite.

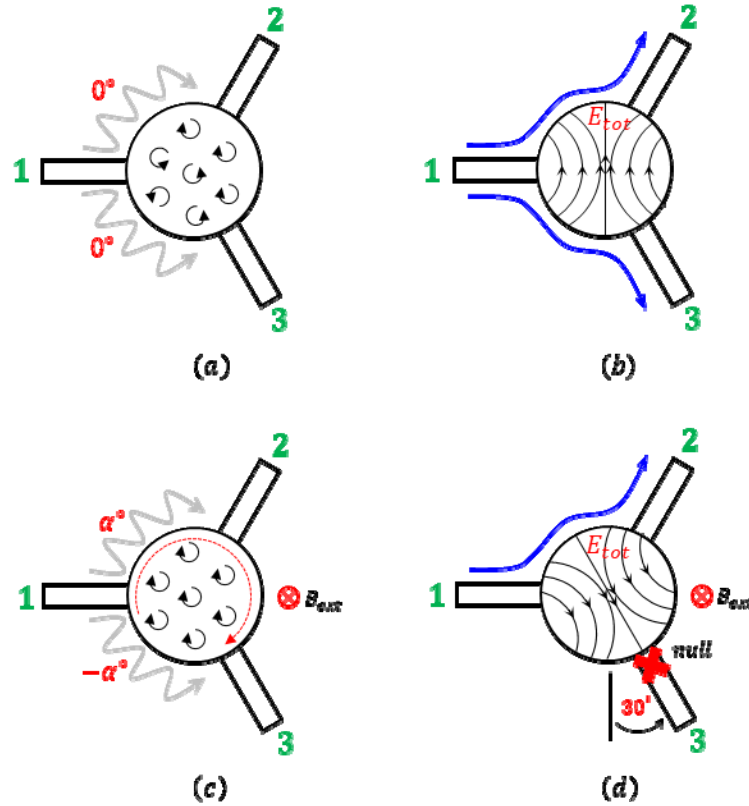


Figure 2: Magnetic circulator. (a) Magnetic dipole moments without bias. (b) Total electric field distribution without bias. (c) Magnetic dipole moments with bias. (d) Total electric field distribution with bias.

We see from the discussion above that the underlying physical principles of cyclic-symmetric circulators are: (i) to ensure that the in-phase mode is zero and (ii) to provide a preferred sense of precession for the counter-rotating modes that alter only their phases but not their amplitudes. In magnetic circulators, this is achieved by applying a magnetic bias to a ferrite cavity, which is symmetrically attached to three ports at 120° intervals, as shown in Fig. 2. Due to charge conservation, or equivalently Kirchoff's current law (KCL), the in-phase mode current must be zero, otherwise charges will continue to accumulate boundlessly inside the cavity, hence the total electric field can be decomposed into a pair of rotating modes with azimuthal dependence $e^{\pm j\varphi}$. Without external bias, the magnetic dipole moments of the spinning electrons inside the ferrite disk are randomly oriented [see Fig. 2(a)] and the counter-rotating modes have the same resonant frequency. As a result, an incident wave at one port, say port 1, excites the counter-rotating modes with the same amplitude and phase, leading to a symmetrical field distribution with respect to the input port. For example, Fig. 2(b) shows the total field distribution for a driving frequency close to the resonance of the cavity. Due to the symmetry of the field distribution and the symmetry of the output ports with respect to the input one, the output signals at ports 2 and 3 are identical, showing that the unbiased junction operates as a symmetrical three-port junction. When a static magnetic bias is applied, however, along the axis of the ferrite cavity, the spinning electrons' dipole moments align in the same direction, as shown in Fig 1(c). At a macroscopic level, this alignment imitates an effective continuous mechanical rotation of the ferrite cavity at a constant speed, since the distance between the microscopic dipole moments is much smaller than the wavelength of the input signals, hence it provides a uniform preferred sense of precession for the counter rotating modes. In this case, the mode that propagates in the same direction of the precession will exhibit a different propagation velocity and,

consequently, a different resonant frequency than the mode that propagates in the opposite direction, showing that the degeneracy of the rotating modes is lifted by the external bias. If the magnetic bias is also uniformly distributed across the cavity's cross section, then the strength of the rotating modes remains identical. Therefore, an incident wave at any port in the middle of the resonant frequencies of the rotating modes will excite them with the same amplitude but with opposite phases $\pm\alpha$, resulting in a rotated electric field pattern, as illustrated in Fig. 2(d). For $\alpha = 30^\circ$, the rotated field pattern has a zero at port 3, resulting in zero transmission at this port, as shown in Fig. 2(d), and transmission of all the input power, assuming negligible losses, from port 1 to port 2. Similarly, for excitation at port 2 or 3, input power is exclusively transmitted to port 3 and 1, respectively.

III. SINGLE-ENDED STM-AM CIRCULATORS

In Sec. II, it was shown that magnetic circulators consist of a three-port resonant cavity, designed to ensure that a non-zero in-phase mode would violate KCL, and a preferred sense of precession is provided uniformly for the rotating modes such that they are excited with the same amplitude but with opposite phases. In light of these remarks, the STM-AM circulators can now be developed as follows. First, the resonant ferrite cavity is replaced by three series or parallel LC tanks connected in a loop or to a central node, which results in four possible combinations, namely, bandpass/wye, bandstop/delta, bandstop/wye, and bandpass/delta, as shown in Fig. 3. These circuits are essentially single-ended implementations of STM-AM circulators and they guarantee that the in-phase mode current is zero because otherwise it would violate KCL. A uniform preferred sense of precession is also provided for the rotating currents by modulating the instantaneous natural oscillation frequencies of the LC tanks through variable capacitors as follows

$$f_n = f_0 + kV_m \cos(\omega_m t + (n-1)2\pi/3), \quad (10)$$

where f_n is the instantaneous oscillation frequency of the n -th tank, f_0 is the static unmodulated oscillation frequency of all tanks, V_m and ω_m are the modulation amplitude and frequency, respectively, and k is a constant with Hz/Volt units that depends on the varactors or switched capacitors used in the implementation. Notice that the phases of the modulation signals increase by 120° in the clockwise direction similar to I_+ and, necessarily, opposite to I_- , however, the modulation depth and frequency are the same for all tanks. Therefore, only the phases of I_\pm become different but their amplitudes remain identical. We refer to this modulation scheme as spatiotemporal modulation angular-momentum (STM-AM) biasing, since it involves phase variation in space (φ direction) and in time (t), which synthesizes an effective angular momentum that mimics the effect of the aligned dipole moments in magnetic-biased ferrite cavities, i.e., both provide uniformly a preferred sense of precession for the rotating modes I_\pm . Therefore, the circuits of Fig. 3 are all expected to yield the functionality of a circulator. It is also worth mentioning that without modulation, both the bandpass/wye and the bandpass/delta topologies operate as a symmetrical three-port bandpass filter, similar to magnetic circulators when no bias is applied. In contrast, the bandstop/delta and the bandstop/wye topologies do not, in fact, allow any transmission between the ports when the modulation is turned OFF. While it does seem counter intuitive, the previous analysis still applies and both circuits do work as magnetless circulators. More specifically, the STM-AM bias lifts the degeneracy of the rotating modes at the resonance frequency $\omega_0 = 1/\sqrt{L_0 C_0}$, therefore when the modulation is applied, the circuit actually oscillates at $\omega_0 \pm \omega_m$ rather than ω_0 . In between these two frequencies, the skirts of the resonances do allow transmission and they exhibit opposite phases. Therefore, if an input signal is incident at one port at the middle of these two frequencies, i.e., at ω_0 , it will excite the two resonances with equal magnitude and opposite phase, thus allowing to achieve isolation at one port and perfect transmission to another. This is consistent with the previous description in in Sec. II based on providing a preferred sense of precession. However, such description assumes

that the effective angular momentum bias is continuous, which is indeed satisfied by the ferrite cavity at a macroscopic level, but which is different in the SE STM-AM circulators of Fig. 3. These circuits consist of three modulated resonators, which results in a discrete staircase approximation of the uniform rotation of the junction. Therefore, large IMPs emerge at all ports, which degrade the overall performance of the circulator as explained in the introduction. Specifically, the bandstop/wye and the bandpass/delta topologies are severely impacted by these mixing products, explaining the limited explorations of these circuits in previous publications on STM-AM circulators. Nevertheless, we include them herein because this problem can be addressed by the differential and the N -way architectures, which will be discussed in Sec. IV and Sec. V, respectively.

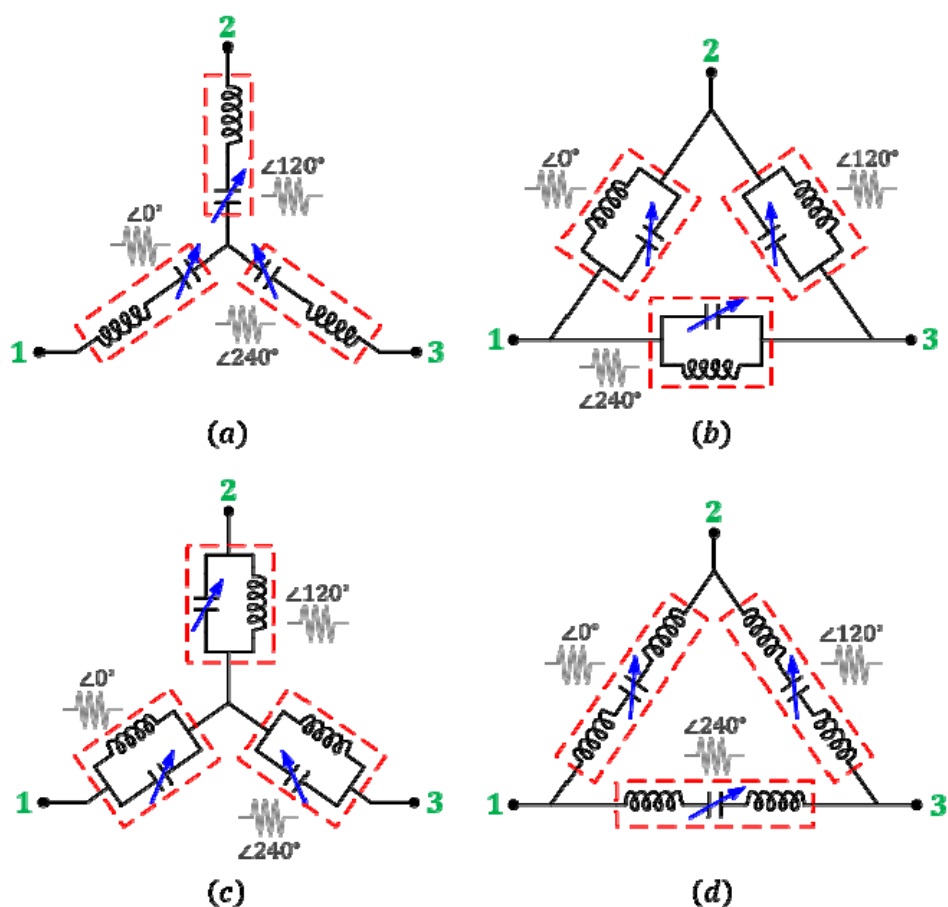


Figure 3: Single-ended STM-AM circulator: (a) Bandpass/wye. (b) Bandstop/delta.
(c) Bandstop/wye. (d) Bandpass/delta.

IV. DIFFERENTIAL STM-AM CIRCULATORS

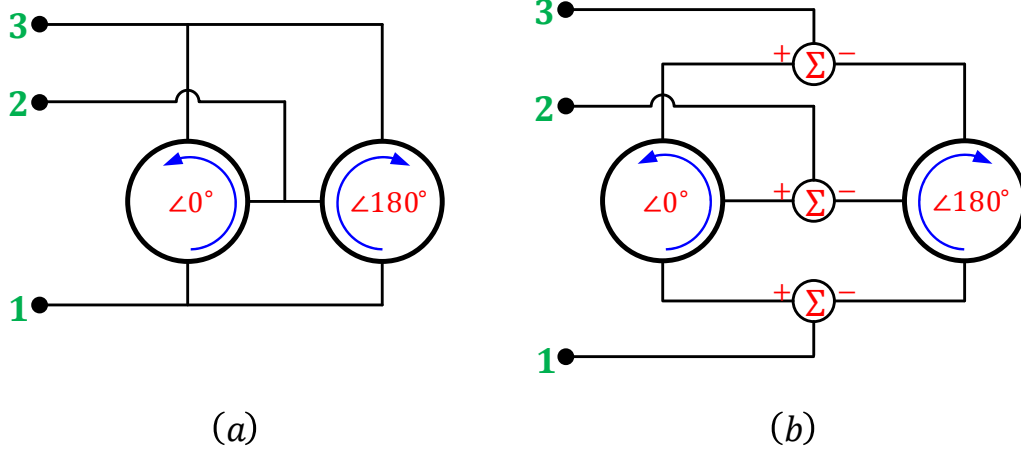


Figure 4: Differential STM-AM circulator: (a) Current-mode. (b) Voltage-mode.

In order to alleviate the spurious emission problem of the SE circuits in Fig. 3, [30] presented a partial solution based on connecting two of these circuits either in parallel or in series (through a subtractor) as shown in Fig. 4(a) and Fig. 4(b), respectively, and modulating the oscillation frequencies of all tanks as

$$f_n = f_0 + kV_m \cos\left(\omega_m t + (n-1)\frac{2\pi}{3} + (i-1)\pi\right), \quad (11)$$

where $i=1:2$ is the index of the SE circuit. In analogy with passive mixers, these differential circuits were called current- and voltage-mode architectures. In the current-mode architecture, the constituent SE circuits are based on either one of the wye topologies in Fig. 3(a) and Fig. 3(c), since the IMPs in this case are expected to arise as differential currents at the input terminals. In the voltage-mode architecture, however, the IMPs are expected to arise as common-mode voltages, hence the SE circuits must be based on one of the delta topologies in Fig. 3(b) and Fig. 3(d). Therefore, there are only four optimal differential implementations of STM-AM circulators, namely current-mode bandpass/wye, current-mode bandstop/wye, voltage-mode bandpass/delta, and voltage-

mode bandstop/delta topologies. Fig. 5 shows a comparison between the S -parameters of these four differential circuits, assuming the same modulation frequency of 221 MHz, capacitance variation of 50%, and unloaded quality factor of 50. These results were obtained using rigorous small-signal analysis, the details of which are provided in [30], together with a rigorous validation with full-wave simulations and measurements. The maximum isolation in all cases exceeds 60 dB, but the insertion loss varies from 0.84 dB to 2 dB, the return loss varies from 17.5 dB to 20.7 dB, and the fractional bandwidth varies from 2.4% to 4%, as summarized in Table I. These results show that the best S -parameters, i.e., lowest insertion loss, largest return loss, largest bandwidth and, consequently, the lowest noise figure, are achieved by the current-mode bandpass/wye topology. However, one problem with this circuit is that the total required inductance is quite large: six 58 nH inductors are needed to achieve the results of Fig. 5(a). This, in turn, increases the overall size and cost of the device, and it considerably complicates a chip-scale implementation. Another problem is that the power handling of this circuit is the lowest among all STM-AM circulator topologies. This is mainly due to the amplification of the incident voltage across the modulated capacitance by the constituent series LC tanks, which strongly triggers its non-linearities. These problems are overcome by the voltage-mode bandstop/delta topology, which reduces the total required inductance to six 1 nH inductors. Moreover, the input voltage is halved among the constituent SE circuits through a subtractor, thus doubling the maximum power handling. The use of parallel LC tanks also increases the power handling, since the incident current is amplified instead of the voltage, but this makes the bandstop/delta topology more sensitive to resistive losses. Nevertheless, the required subtractors in this case, implemented using baluns or transformers, incur additional losses of about 0.5 dB. In summary, the current-mode bandpass/wye topology is optimal to achieve the lowest possible insertion loss, while the voltage-mode bandstop/delta topology is optimal to achieve the smallest form factor and largest power handling. A good compromise between all these metrics is offered by the two new topologies presented in this paper, i.e., the current-mode bandstop/wye and the voltage-mode bandpass/delta. The current-

mode bandstop/wye circuit, in particular, can achieve excellent insertion loss and good power handling at a small form factor, hence it would be optimal for general-purpose applications.

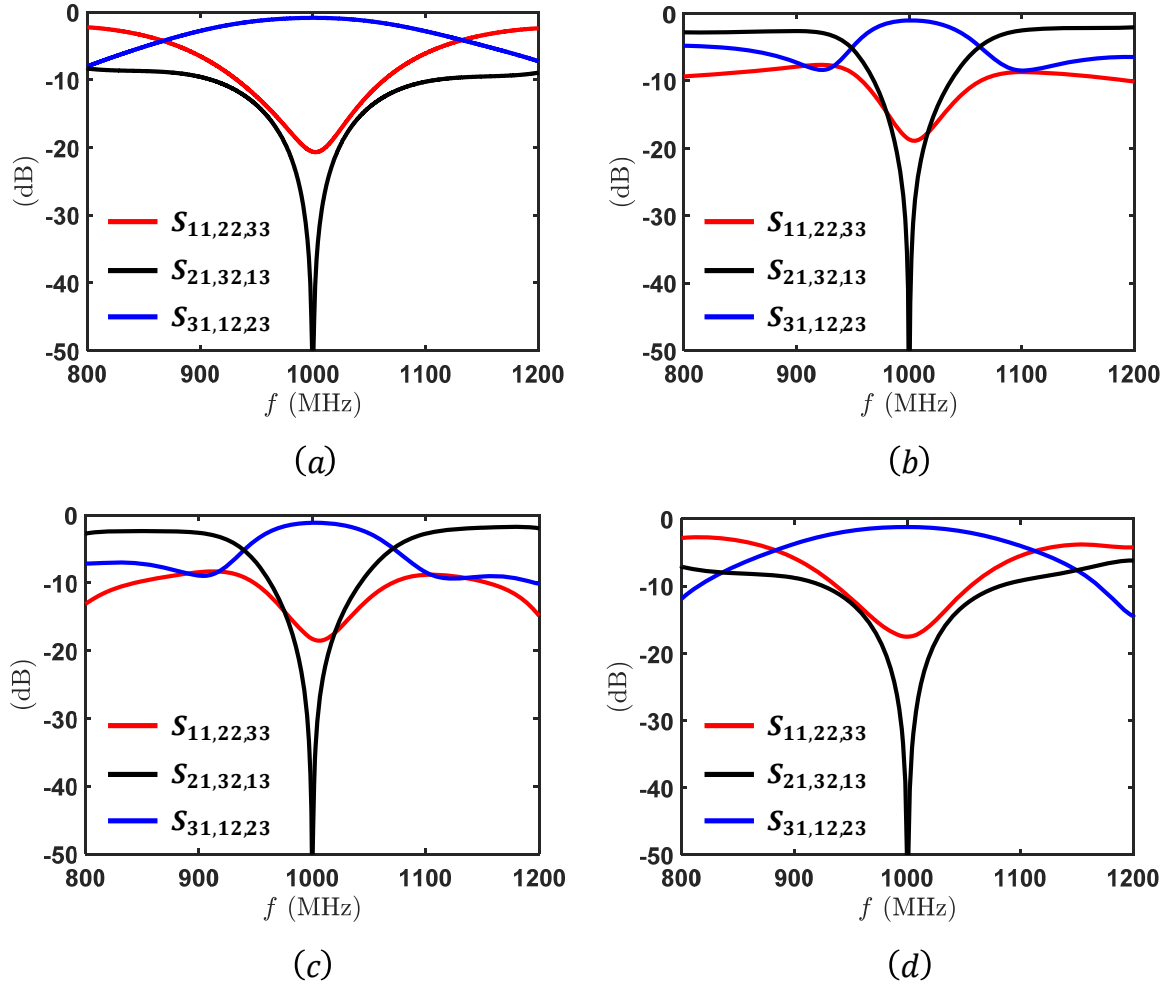


Figure 5: S-parameters: (a) Current-mode bandpass/wye. (b) Voltage-mode bandstop/delta. (c) Current-mode bandstop/wye. (d) Voltage-mode bandpass/delta.

In theory, differential STM-AM circulators have been shown [30] to cancel all IMPs at all ports for input excitation at any frequency, making them QLTI networks. In other words, they synthesize an effective continuous angular momentum bias. This result,

however, was found under several assumptions: (i) the involved components are all linear, (ii) the in-phase mode is zero, (iii) the modulation scheme is sinusoidal, (iv) the constituent SE circuits are identical and perfectly balanced, and (v) all phases are accurately synchronized. In reality, these assumptions are nearly impossible to be satisfied. For instance, if varactors are used to achieve the modulation, the CV characteristics of such pn junctions are known to be exponentially non-linear, which violates the first assumption. Similarly, switched capacitors exhibit strong non-linearity due to the switches' non-linear on-resistance and off-capacitance. Furthermore, the capacitance variation of switched capacitors is quantized, which produces finite IMPs of all orders regardless of the elements' linearity. On the other hand, inevitable layout asymmetries, parasitics and random variations in the elements, and phase errors between the modulation signals, can easily perturb the differential balance and further contribute to the generation of finite spurs. Lastly, the modulation signals themselves, or their higher-order harmonics resulting from non-linearities, may also leak to any of the circulator's ports, thus contaminating the spectrum even more. These remarks are manifested in Fig. 6, which depicts the simulated spectrums from DC to 2 GHz at the antenna and receiver ports of the voltage-mode bandstop/delta topology for a monochromatic transmitter excitation with an input frequency f_m of 1 GHz and an input power P_m of 0 dBm. These results were experimentally validated in [30], showing excellent agreement between simulations and measurements, hence they will be used as a reference in the rest of this paper to show the improvements introduced by the N -way circuits. Clearly, the spectrums are contaminated with many spurs, the largest of which are about -21 dBc at f_m and -25 dBc at $3f_m$, where $f_m = 100$ MHz. These are essentially the modulation leakage and its third-order harmonic, respectively. Also, the second-order harmonic at $2f_m$ is -34 dBc. On the other hand, several of the IMPs at $f_m \pm kf_m$ are also

quite large. Specifically, the second-order spurs at $f_{in} - f_m$ and $f_{in} + f_m$ are -41 dBc and -30 dBc, respectively, the third-order spurs at $f_{in} - 2f_m$ and $f_{in} + 2f_m$ are -30 dBc and -27 dBc, respectively, the fourth-order spurs at $f_{in} - 3f_m$ and $f_{in} + 3f_m$ are -41 dBc and -38 dBc, respectively, and the fifth-order spurs at $f_{in} - 4f_m$ and $f_{in} + 4f_m$ are -41 dBc and -40 dBc, respectively. The rest of the IMPs are all less than -54 dBc and, at the same time, are sufficiently far from the circulator's center frequency $f_{ctr} = f_{in}$, therefore, they can be rejected with filters. Similarly, the modulation leakage and its high-order harmonics can be filtered out. Nevertheless, the necessity of using filters to reject these spurs is in general a drawback as it increases the overall size and cost considerably. Furthermore, the first few IMPs are much more challenging to be filtered out since they are closer to f_{ctr} .

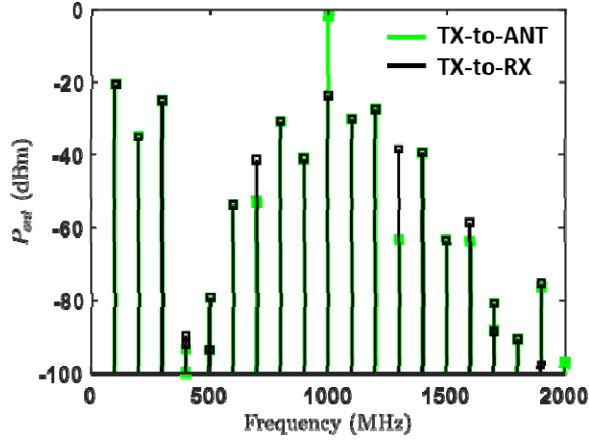


Figure 6: Spurious emission at the antenna and receiver ports of a voltage-mode bandstop/delta topology for a monochromatic transmitter excitation with an input frequency f_{in} of 1 GHz and an input power P_{in} of 0 dBm.

TABLE I
COMPARISON BETWEEN ALL FOUR TOPOLOGIES OF DIFFERENTIAL STM-AM
CIRCULATORS.

Metric\Circuit	Current-mode		Voltage-mode	
	Bandpass /we	Bandstop /we	Bandpass /delta	Bandstop /delta
Isolation (dB)	>+60			
Insertion loss (dB)	0.84	1.1	2 *	1.8 *
Return loss (dB)	20.7	18.5	17.5	18.9
Bandwidth (%)	4.64	2.8	4.6	2.4
Inductance (nH)	6×58.1	6×1.77	6×100	6×1
Power handling	Lowest	Medium	Medium	Highest
Noise figure (dB)	≈ Insertion loss			

* Subtractor losses are included.

V. *N*-WAY STM-AM CIRCULATORS

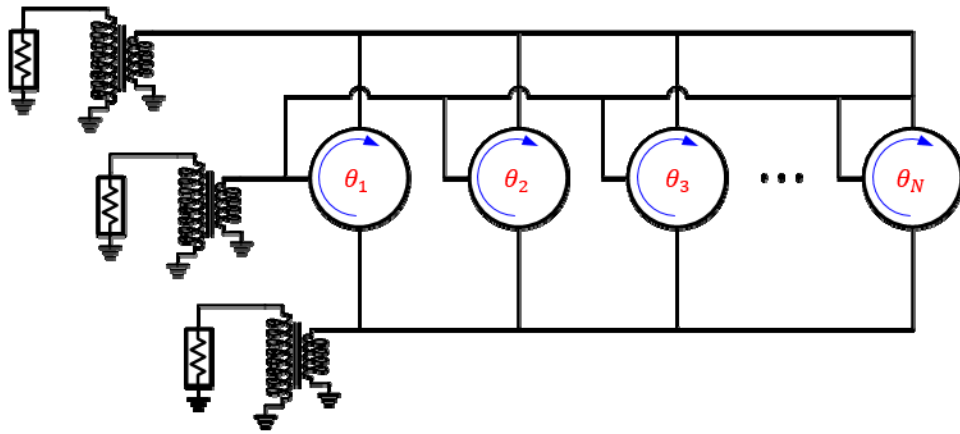
In order to overcome the above problems, we introduce herein a generalization of the differential architectures into *N*-way STM-AM circulators, which consist of *N* circulator units, connected in parallel or in series (through power dividers/combiners) as shown in Fig. 7(a) and Fig. 7(b), respectively, and modulated with the rotating scheme

$$f_n = f_0 + kV_m \cos\left(\omega_m t + (n-1)\frac{2\pi}{3} + (i-1)\frac{2\pi}{N}\right), \quad (12)$$

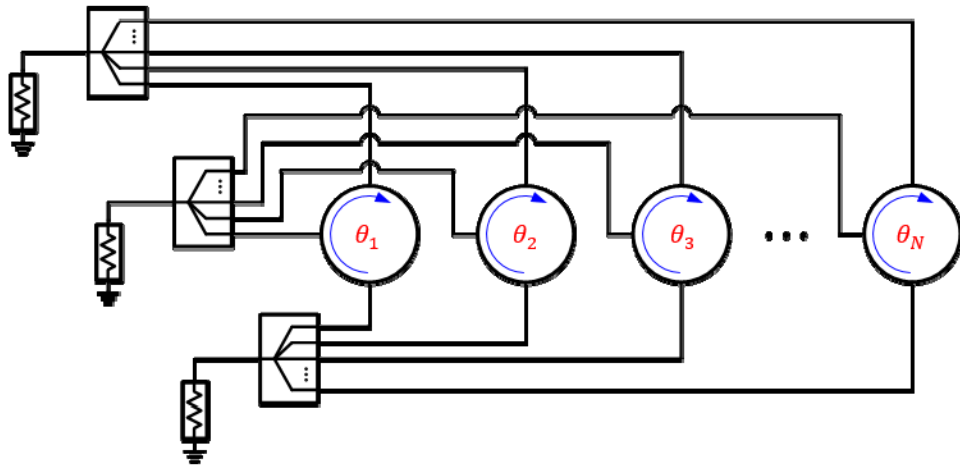
where $i=1:N$ is the unit index. To simplify the design procedure of such circuits, the unit circulator is assumed to be differential rather than SE. The reason is that the IMPs of the differential circuit are already below a sufficient level, i.e., -30 dBc, which guarantees that the *S*-parameters of all units, when interconnected together, are not perturbed by loading effects. In other words, IMPs of different orders do not interact with each other and the impact of their cancellation on the fundamental harmonic is minimal,

hence the overall S -parameters of the combined network remain almost identical to those of the unit element. This, in turn, simplifies the design procedure of the N -way circuit by allowing to optimize the individual unit element separately. Hence, the operation of the N -way circulator can be explained by tracking the individual transmissions through the already-known stages as follows. First, the input power is split amongst N paths, either through a transformer followed by a current splitter (which is simply a common node combining the corresponding terminals of the constituent unit circuits) as in Fig. 7(a), or through a power divider/combiner, as in Fig. 7(b). The N portions of the input signal are then routed by the identical circulator units in the same direction, while exhibiting the same dispersion. Finally, the signals are summed up again at the output ports. Notice that the impedance transformers in Fig. 7(a) must have a down conversion ratio of \sqrt{N} in order to match the Z_0 ports to the Z_0/N impedance of the parallel-interconnected units. In Fig. 7(b), however, the units are combined through power dividers/combiners that can be matched at all ports to Z_0 , hence impedance transformation is not required. Based on this discussion, we reckon that the overall power handling increases by $3 \log_2 N$ dB (Nx in linear scale). On the other hand, thanks to the phase modulation pattern (12) and symmetry considerations, the IMPs at $kf_{in} \pm lf_m$, where f_{in} and f_m are the input and modulation frequencies, respectively, and k and l are positive integers, exhibits a phase increment of $l \times (i-1) 2\pi/N$ at the i -th branch. Therefore, the summation of these products at any port is proportional to $\sum_{i=1}^N e^{j[l \times (i-1) 2\pi/N]}$, which yields zero for any l that is not a multiple integer of N . In other words, in N -way circulators IMPs occur at an Nf_m interval from f_{in} . In order to validate these physical insights, in the following we compare the performance of a 1-way, a 2-way, a 4-way, and an 8-way STM-AM circulator, based on the schematic of Fig. 7(a). The required impedance transformers for $N \neq 1$ are built using a CLC π -section of a $\lambda/4$ TL transformer. Also, in all cases, the unit element is built using the voltage-mode bandstop/delta topology experimentally

validated in [30], showing excellent agreement between the simulated and measured results of all relevant metrics. Therefore, we render simulations sufficient to validate the N -way circuits presented in this paper. It is worth emphasizing that in obtaining the following results, we extracted the layout parasitics using a full-wave simulation and combined them with commercially available full non-linear spice models of all involved elements to perform circuit/EM co-simulations in Keysight ADS. Furthermore, we introduced a random phase error in the phases of (12) with a maximum value of $\pm 5^\circ$ to account for inevitable desynchronization of the modulation signals in practice.



(a)



(b)

Figure 7: N -way STM-AM circulator: (a) Parallel interconnection. (b) Series interconnection.

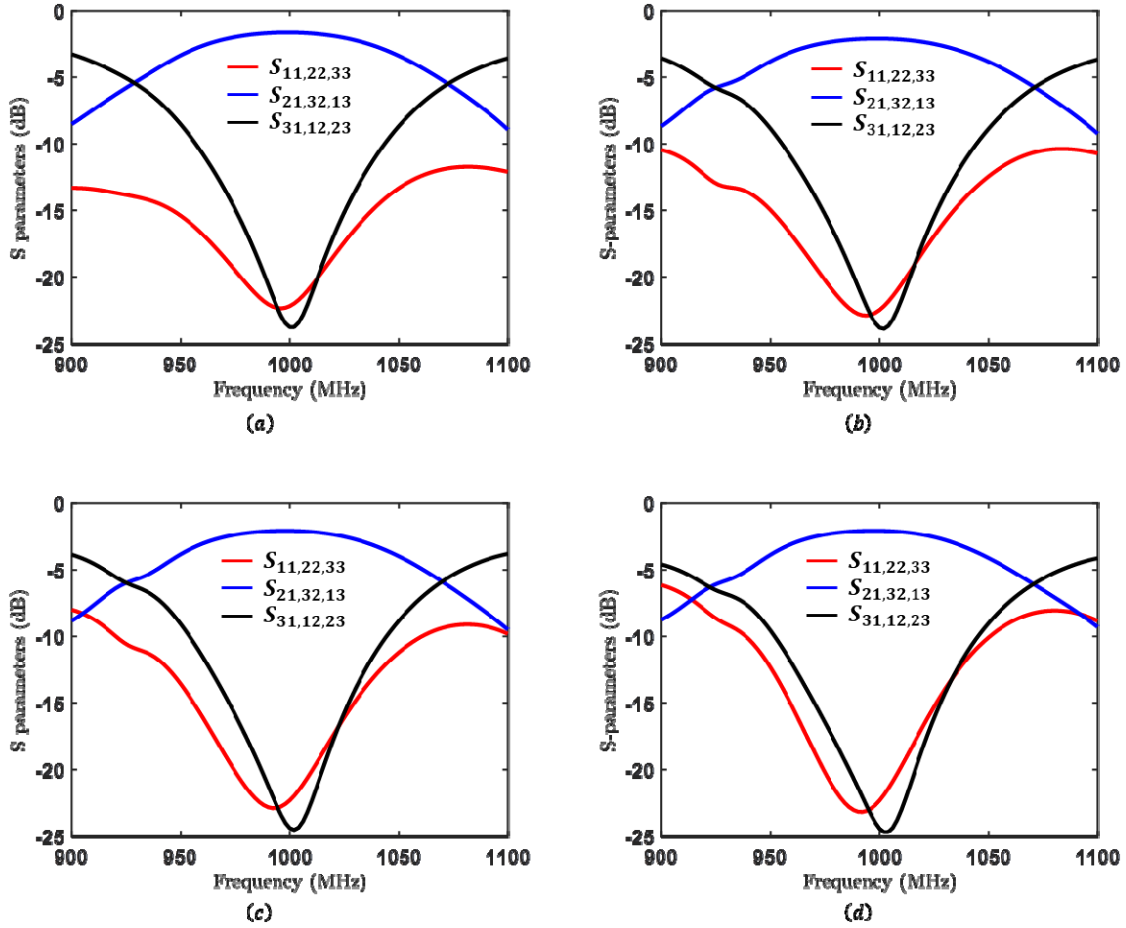


Figure 8: S -parameters. (a) 1-way. (b) 2-way. (c) 4-way. (d) 8-way.

Fig. 8 shows the S -parameters of all 1-way, 2-way, 4-way, and 8-way circuits. The insertion loss, return loss, and isolation of the 1-way circuit at the center frequency $f_{ctr} = 1$ GHz are 1.7 dB, 22 dB, and 24 dB, respectively. The 2-way, 4-way, 8-way circulators all result in nearly the same values of return loss and isolation but insertion loss increases to 2.2 dB at f_{ctr} due to the additional losses incurred by the impedance transformers. Such transformers also change the dispersion of the S -parameters, particularly return loss

and isolation, thus increasing the bandwidth from 2.3% (23 MHz) in the 1-way circuit to 2.6% (26 MHz) in the 2-way circuit and finally to 3% (30 MHz) in both the 4-way and 8-way circuits. It is also worth mentioning that these circuits were intentionally designed to minimize the dispersion of isolation over the desired bandwidth rather than maximizing its value at the center frequency, which is more relevant in practice [30].

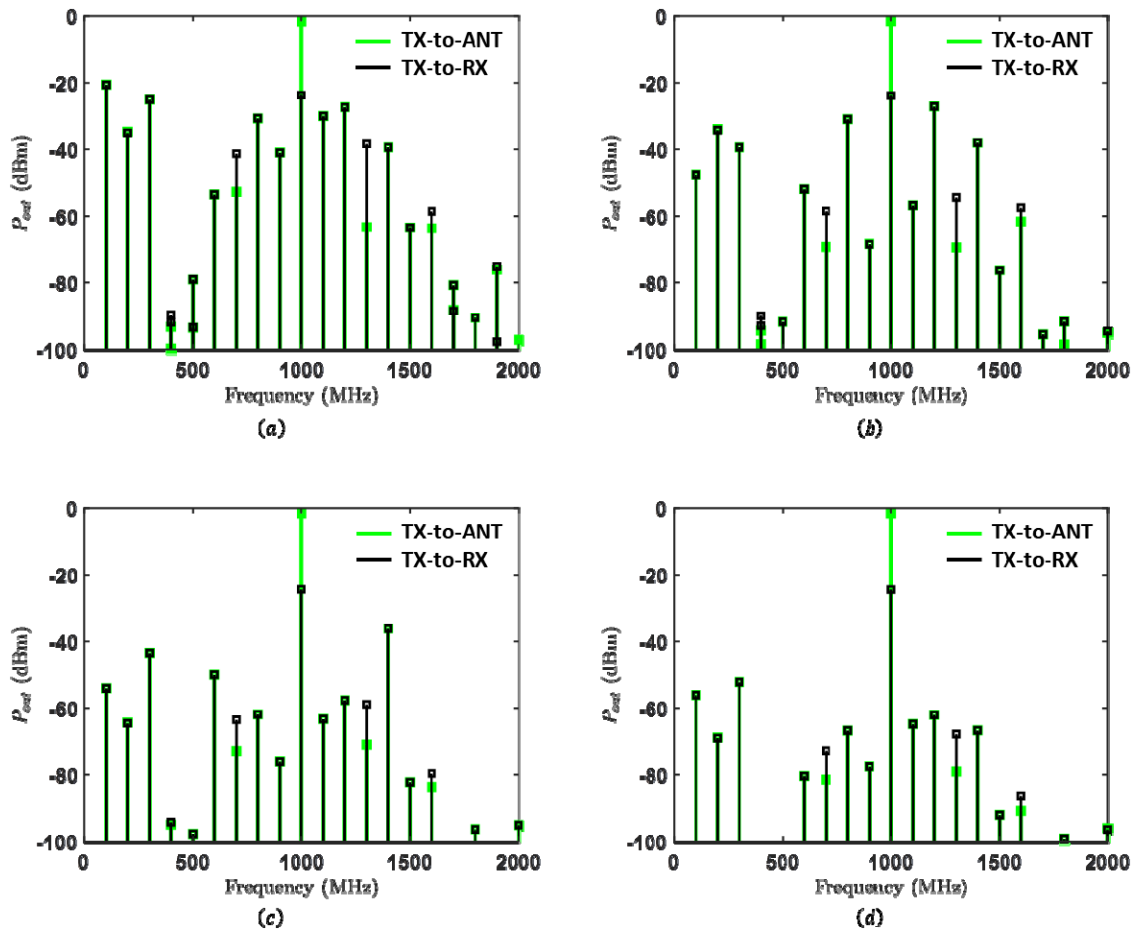


Figure 9: Output spectrums at the antenna and the receiver ports for a harmonic excitation at the transmitter port with a frequency f_{ctr} . (a) 1-way. (b) 2-way. (c) 4-way. (d) 8-way.

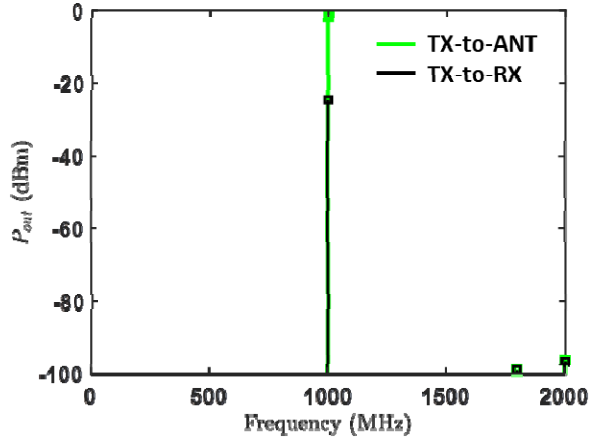


Figure 10: Output spectrum at the antenna and the receiver ports of an 8-way circulator for a harmonic excitation at the transmitter port with a frequency f_{ctr} , assuming perfect synchronization of all modulation signals and identical constituent elements.

Fig. 9 also shows the spectra at both the antenna and receiver ports for a monochromatic transmitter excitation with an input frequency f_{in} of 1 GHz and an input power P_{in} of 0 dBm. As explained earlier, finite spurs of all orders arise due to the inevitable phase errors, device mismatches, and layout asymmetries, which cannot be avoided in reality. For example, the first few even-order IMPs of the 1-way circuit at $f_{in} \pm f_m$, $f_{in} \pm 3f_m$, and $f_{in} \pm 5f_m$ range from -53 dBc to -30 dBc, as shown in Fig. 9(a). If all non-idealities were neglected, however, these IMPs would asymptotically approach zero since the 1-way circuit is a differential implementation itself. In order to approach this ideal result in practice, the differential connection can be repeated. For example, the 2-way circulator which is essentially a differential circuit of differential unit cells adds 25 dB more suppression to the same IMPs, as shown in Fig. 9(b). The modulation leakage at f_m is also reduced from -21 dBc to -48 dBc and the third-order harmonic at $3f_m$ is reduced from -25 dBc to -48 dBc. Nevertheless, the odd-order IMPs, including the large

spurs at $f_{in} \pm 2f_m$, and the second-order harmonic of the modulation signals at $2f_m$ are almost not impacted. In fact, these spurs increase by about 1~3 dB compared to the 1-way circuit because of the aforementioned non-idealities. This problem is solved by the 4-way circulator which reduces the IMPs at $f_{in} \pm 2f_m$ to -58 dBc and the second-order harmonic of the modulation signals at $2f_m$ to -65 dBc, as shown in Fig. 9(c). Notice that the IMPs at $f_{in} \pm 4f_m$ are almost not affected, as expected. These spurs can be suppressed by the 8-way circulator which maintains all IMPs and modulation leakage spurs below -60 dBc and -50 dBc, respectively, as shown in Fig. 9(d). As one may expect, a 16-way circulator would clean the spectrums even further, but this comes at the expense of increasing the overall size and the power consumed in generating the modulation signals considerably, therefore an 8-way circulator is arguably the optimal choice in reality. Also, as mentioned earlier, the performance of an N -way circulator, for a given N , would automatically improve if the layout symmetry is enhanced and the phase relation of (12) is tightly enforced. For example, Fig. 10 shows the spectrums at the antenna and the receiver ports when the modulation phases are perfectly synchronized and the constituent 8 unit elements become identical. Obviously, the results dramatically improve and all spurs are entirely eliminated, thus making this circuit truly an LTI device that would be useful for a variety of applications, as mentioned in the introduction.

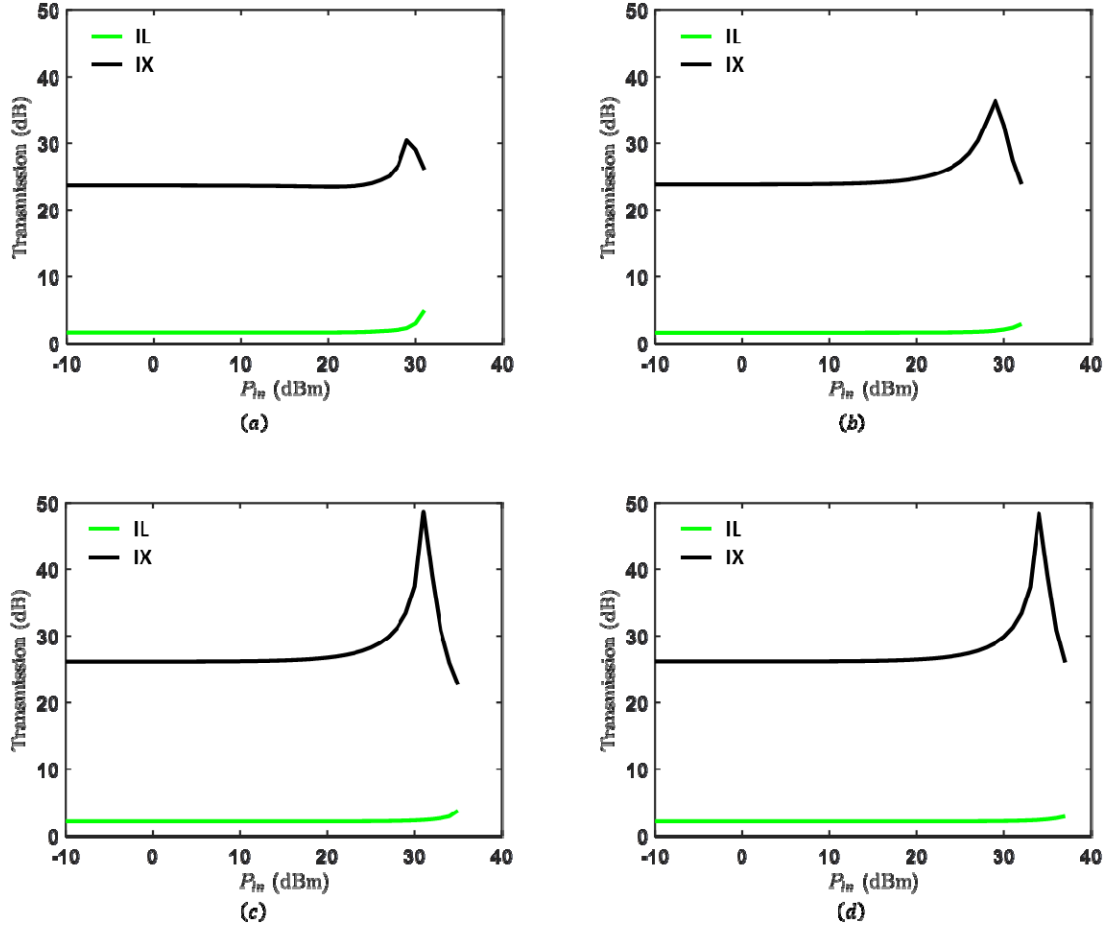


Figure 11: Insertion loss (IL) and isolation (IX) compression versus input power (P_{in}) of a harmonic excitation with a frequency f_{ctr} . (a) 1-way. (b) 2-way. (c) 4-way. (d) 8-way.

Fig. 11 shows the insertion loss and isolation versus input power P_{in} . Both metrics compress at large values of P_{in} , hence the maximum possible input power (Pmax) can be defined as follows

$$P_{max} = \min \{ P1_{dB}, IX20_{dB} \}, \quad (13)$$

where P_{1dB} is the 1 dB input compression point of insertion loss and IX_{20dB} is the 20dB input compression point of isolation. The 1-way, 2-way, 4-way, and 8-way circulators result in P_{max} of +30 dBm, +33 dBm, +36 dBm, and +39 dBm, respectively. As expected, P_{max} increases by +3 dB for each doubling of the unit elements. It is also worth mentioning that P_{max} is in general frequency dependent; hence a spectral average of (13) over the desired bandwidth may be used instead for input signals with finite bandwidth. Also, a back-off value may be considered for long-term reliability of the device.

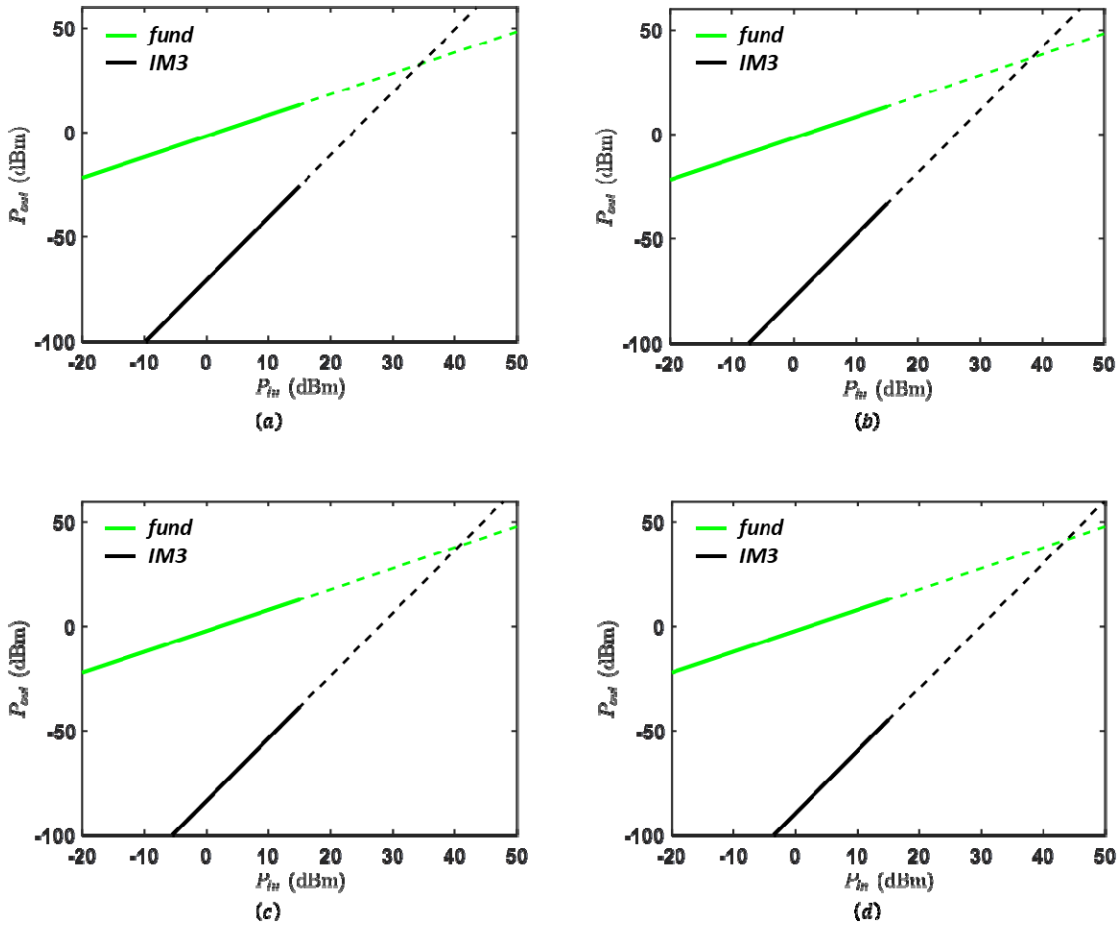


Figure 12: Output power (P_{out}) of the fundamental component (fund) and the third-order harmonic (IM3) versus input power (P_{in}) of a two-tone excitation with a 10 MHz separation around f_{ctr} . (a) 1-way. (b) 2-way. (c) 4-way. (d) 8-way.

Fig. 12 also shows the output power at the antenna port for a two-tone excitation at the transmitter port, each at 0 dBm and separated by 1 MHz. The input-referred third-order intercept point (IIP3) achieved by the 1-way, 2-way, 4-way, and 8-way circulators are +34 dBm, +37 dBm, +40 dBm, +43 dBm, respectively.

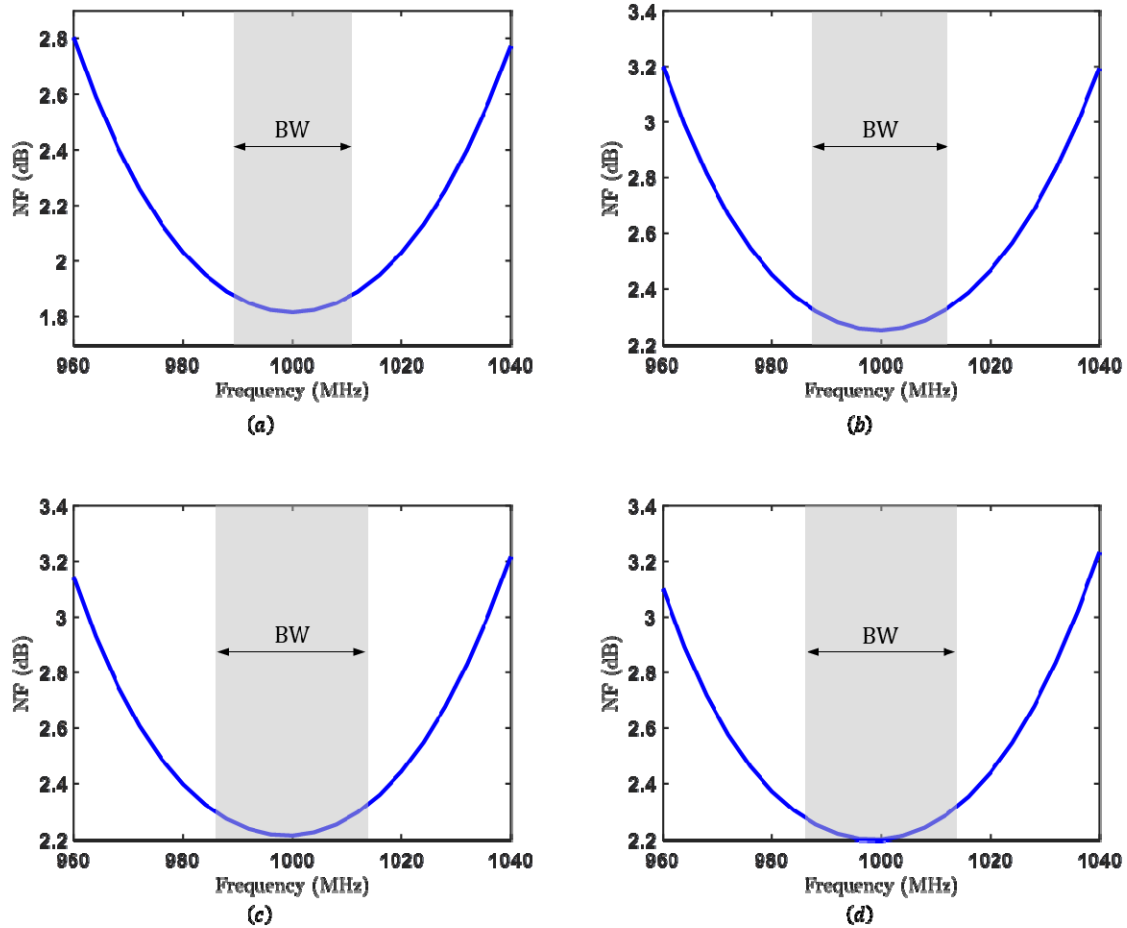


Figure 13: Noise figure. (a) 1-way. (b) 2-way. (c) 4-way. (d) 8-way.

Finally, Fig. 13 shows the receiver noise figure. The minimum noise figure of the 1-way circulator, at the center frequency of 1 GHz, is 1.8 dB and it increases to 1.9 dB at the edges of the 2.3% bandwidth (highlighted in grey). On the other hand, the 2-way circuit results in a minimum noise figure of 2.25 dB at 1 GHz and it increases to 2.35 dB

at the edges of the 2.6% bandwidth. Also, the 4-way and 8-way circulators both result in a minimum noise figure of 2.2 dB at 1 GHz and it increases to 2.3 dB at the edges of the 3% bandwidth. Similar to the insertion loss, noise figure of the 2-way, 4-way and 8-way circuits is larger than that of the 1-way circuit because of the additional losses incurred by the impedance transformers. Also, noise figure of the 4-way and 8-way circulators results is identical to the insertion loss, thanks to the drastic reduction of the IMPs which, in turn, reduces the noise folding into the fundamental bandwidth.

TABLE II
SUMMARY OF RESULTS.

Metric\Circulator	1-way	2-way	4-way	8-way
Cent. freq. (MHz)	1000	1000	1000	1000
Mod. freq. (%)	10	10	10	10
Bandwidth (%)	2.3	2.6	3	3
Isolation (dB) †	>20	>20	>20	>20
Insertion loss (dB) †	<1.8	<2.3	<2.3	<2.3
Return loss (dB) †	>20	>20	>20	>20
P1dB (dBm)	+30	+33	+36	+39
IX20dB (dBm)	+32	+35	+38	+41
IIP3 (dBm)	+34	+37	+40	+43
Noise figure (dB) †	<2.35	<2.33	<2.3	<2.3
IMPs (dBc)	-27 @ $f_0 \pm 2f_m$	-27 @ $f_0 + 2f_m$	-36 @ $f_0 + 4f_m$	<-62
	-30 @ $f_0 - 2f_m$ & $f_0 + f_m$	-31 @ $f_0 - 2f_m$	-50 @ $f_0 - 4f_m$	
Mod. leakage (dBc)	-21 @ f_m	-34 @ $2f_m$	-44 @ $3f_m$	-52 @ $3f_m$
	-25 @ $3f_m$	-40 @ $3f_m$	-54 @ f_m	-56 @ f_m
	-35 @ $2f_m$	-47 @ f_m	-65 @ $2f_m$	-69 @ $2f_m$

† Over the bandwidth.

For convenience, the previous results are all summarized in Table II. It is also worth mentioning that the bandwidth extension technique proposed in [31] can be applied to the presented N -way circuits in a straightforward manner to enhance the bandwidth

performance of the circuit using simply passive matching networks. Also, varactors can be replaced by switched capacitors, which reduces the complexity without degrading the performance, since the IMPs resulting from the quantized modulation scheme would also be cancelled by the N -way interconnection. Therefore, we argue that an IC STM-AM magnetless can be designed using conventional CMOS processes at low cost and small size while maintaining an excellent performance in all metrics.

VI. CONCLUSIONS

In this paper, we demonstrated that a network of N -interconnected STM-AM circuits with a rotating phase pattern of their modulation signals, imparts an effect analogous to a continuous angular momentum bias, despite the discretized modulation of the unit elements and their associated non-linearities. This is consistent with the effective macroscopic precession of the ferrite cavity in magnetic circulators and the uniform mechanical rotation of a fluid inside an acoustic cavity presented in [47]. This, in turn, allows the proposed N -way circuits to increase the power handling by a factor of N and to realistically suppress the spurious emission below a sufficient level dictated by real-life standards. In other words, from a terminal perspective, the N -way circuits look like a linear time-invariant system even though the individual elements are non-linear and time-varying. We validated these circuits by comparing the results of a 1-way, a 2-way, a 4-way, and an 8-way circulator in the presence of all practical non-idealities, including finite non-linearities of the modulating elements, timing errors, and device mismatches. The results show that an 8-way circulator can handle up to 8 Watt input power and maintain the mixing IMPs below -60 dBc, which exceeds the performance of all magnetless circulators presented to date by orders of magnitude. We believe that this generalization of the STM-AM approach opens exciting opportunities to realize superior non-reciprocal devices meeting the specifications of real-life applications ranging from wireless communications to quantum computing.

ACKNOWLEDGMENTS

This work was supported by the DARPA SPAR program, the Air Force Office of Scientific Research and the National Science Foundation.

REFERENCES

- [1] D. Korpi, J. Tamminen, M. Turunen, T. Huusari, Y. S. Choi, L. Anttila, S. Talwar, and M. Valkama, “Full-duplex mobile device: pushing the limits,” *IEEE Commun. Mag.* **54**, 80 (2016).
- [2] A. Sabharwal, P. Schniter, D. Guo, D. W. Bliss, S. Rangarajan, and R. Wichman, “In-Band Full-Duplex Wireless: Challenges and Opportunities,” *IEEE J. Sel. Areas Commun.* **32**, 1637–1652 (2014).
- [3] B. Debaillie, D. van den Broek, C. Lavín, B. van Liempd, E. A. M. Klumperink, C. Palacios, J. Craninckx, B. Nauta, and A. Pärssinen, “Analog/RF Solutions Enabling Compact Full-Duplex Radios,” *IEEE J. Sel. Areas Commun.* **32**, 1662 (2014).
- [4] D. Bharadia, E. Mcmilin, and S. Katti, “Full duplex radios,” *ACM SIGCOMM Comput. Commun. Rev.* **43**, 375 (2013).
- [5] M. Duarte, C. Dick, and A. Sabharwal, “Experiment-driven characterization of full-duplex wireless systems,” *IEEE Trans. Wireless Commun.* **11**, 4296 (2012).
- [6] J. Zhou, N. Reiskarimian, J. Diakonikolas, T. Dinc, T. Chen, G. Zussman, and H. Krishnaswamy, “Integrated full duplex radios,” *IEEE Commun. Mag.* **55**, 142 (2017).
- [7] A. Kord, D. L. Sounas, and A. Alù, “Achieving Full-Duplex Communication: Magnetless Parametric Circulators for Full-Duplex Communication Systems,” *IEEE Microw. Mag.* **19**, 84 (2018).
- [8] C. M. Caves, “Quantum limits on noise in linear amplifiers,” *Phys. Rev. D* **26**, 1817 (1982).
- [9] A. A. Clerk, M. H. Devoret, S. M. Girvin, F. Marquardt, and R. J. Schoelkopf, “Introduction to quantum noise, measurement, and amplification,” *Rev. Mod. Phys.* **82**, 1155 (2010).
- [10] A. Kamal, J. Clarke, and M. H. Devoret, “Noiseless non-reciprocity in a parametric active device,” *Nat. Phys.* **7**, 311 (2011).
- [11] J. Kerckhoff, K. Lalumière, B. J. Chapman, A. Blasi, and K. W. Lehnert, “On-Chip Superconducting Microwave Circulator from Synthetic Rotation,” *Phys. Rev. Appl.* **4**, 034002 (2015).
- [12] K. M. Sliwa, M. Hatridge, A. Narla, S. Shankar, L. Frunzio, R. J. Schoelkopf, and M. H. Devoret, “Reconfigurable Josephson Circulator/Directional Amplifier,” *Phys. Rev. X* **5**, 041020 (2015).
- [13] F. Lecocq, L. Ranzani, G. A. Peterson, K. Cicak, R. W. Simmonds, J. D. Teufel, and J. Aumentado, “Nonreciprocal Microwave Signal Processing with a Field-Programmable Josephson Amplifier,” *Phys. Rev. Appl.* **7**, 024028 (2017).
- [14] A. A. Clerk, M. H. Devoret, S. M. Girvin, F. Marquardt, and R. J. Schoelkopf, “Introduction to quantum noise, measurement, and amplification,” *Rev. Mod. Phys.* **82**, 1155 (2010).

- [15] E. I. Rosenthal, B. J. Chapman, A. P. Higginbotham, J. Kerckhoff, and K. W. Lehnert, "Breaking Lorentz reciprocity with frequency conversion and delay," *Phys. Rev. Lett.* **119**, 147703 (2017).
- [16] K. M. Sliwa, M. Hatridge, A. Narla, S. Shankar, L. Frunzio, R. J. Schoelkopf, and M. H. Devoret, "Reconfigurable Josephson circulator/directional amplifier," *Phys. Rev. X* **5**, 041020 (2015).
- [17] B. K. O'Neil and J. L. Young, "Experimental investigation of a self-biased microstrip circulator," *IEEE Trans. Microw. Theory Techn.* **57**, 1669 (2009).
- [18] A. Saib, M. Darques, L. Piraux, D. Vanhoenacker-Janvier, and I. Huynen, "Unbiased microwave circulator based on ferromagnetic nanowires arrays of tunable magnetization state," *J. Phys. D, Appl. Phys.* **38**, 2759 (2005).
- [19] L. P. Carignan, A. Yelon, D. Menard, and C. Caloz, "Ferromagnetic nanowire metamaterials: Theory and applications," *IEEE Trans. Microw. Theory Techn.* **59**, 2568 (2011).
- [20] S. A. Oliver, P. Shi, W. Hu, H. How, S. W. McKnight, N. E. McGruer, P. M. Zavaracky, and C. Vittoria, "Integrated self-biased hexaferrite microstrip circulators for millimeter-wavelength applications," *IEEE Trans. Microw. Theory Techn.* **49**, 385 (2001).
- [21] J. Wang, A. Yang, Y. Checn, Z. Chen, A. Geiler, S. M. Gillette, V. G. Harris, and C. Vittoria, "Self-biased Y-junction circulator at Ku band," *IEEE Microw. Wireless Compon. Lett.* **21**, 292 (2011).
- [22] T. Kodera, D. L. Sounas, and C. Caloz, "Magnetless nonreciprocal metamaterial (MNM) technology: application to microwave components," *IEEE Trans. Microw. Theory Techn.* **61**, 1030 (2013).
- [23] T. Kodera, D. L. Sounas, and C. Caloz, "Artificial Faraday rotation using a ring metamaterial structure without static magnetic field," *Appl. Phys. Lett.* **99**, 031114 (2011).
- [24] S. Wang, C. H. Lee, and Y. B. Wu, "Fully Integrated 10-GHz Active Circulator and Quasi-Circulator Using Bridged-T Networks in Standard CMOS," *IEEE Trans. Very Large Scale Integr. (VLSI) Sys.* **24**, 3184 (2016).
- [25] C.-H. Chang, Y.-T. Lo, and J.-F. Kiang, "A 30 GHz active quasicirculator with current-reuse technique in 0.18 μm CMOS technology," *IEEE Microw. Wireless Compon. Lett.* **20**, 693 (2010).
- [26] G. Carchon and B. Nanwelaers, "Power and noise limitations of active circulators," *IEEE Trans. Microw. Theory Techn.* **48**, 316 (2000).
- [27] N. A. Estep, D. L. Sounas, J. Soric, A. Alù, "Magnetic-free non-reciprocity and isolation based on parametrically modulated coupled-resonator loops," *Nat. Phys.* **10**, 923 (2014).
- [28] N. A. Estep, D. L. Sounas, and Andrea Alù, "Magnetless Microwave Circulators Based on Spatiotemporally Modulated Rings of Coupled Resonators," *IEEE Trans. Microw. Theory Techn.* **64**, 502 (2016).
- [29] A. Kord, D. L. Sounas, and A. Alù, "Magnetless Circulators Based on Spatio-Temporal Modulation of Bandstop Filters in a Delta Topology," *IEEE Trans. Microw. Theory Techn.* **66**, 911 (2018).

- [30] A. Kord, D. L. Sounas, and A. Alù, "Pseudo-Linear Time-Invariant Magnetless Circulators Based on Differential Spatio-Temporal Modulation of Resonant Junctions," *IEEE Trans. Microw. Theory Techn.* **66**, 2731 (2018).
- [31] A. Kord, D. L. Sounas, Z. Xiao, and A. Alù, "Broadband Cyclic-Symmetric Magnet-less Circulators and Theoretical Bounds on their Bandwidth," *IEEE Trans. Microw. Theory Techn.* **66**, 5472 (2018).
- [32] A. Kord, M. Tymchenko, D. L. Sounas, H. Krishnaswamy, A. Alù, "CMOS Integrated Magnetless Circulators Based on Spatiotemporal Modulation Angular-Momentum Biasing," *IEEE Trans. Microw. Theory Techn.* **67**, 2649 (2019).
- [33] D. L. Sounas, N. A. Estep, A. Kord, and A. Alù, "Angular-Momentum Biased Circulators and Their Power Consumption," *IEEE Antennas Wireless Propag. Lett.* **17**, 1963 (2018).
- [34] A. Kord, D. L. Sounas, and A. Alù, "Differential Magnetless Circulator Using Modulated Bandstop Filters," in *Proc. IEEE MTT-S Int. Microw. Symp. (IMS)*, Honolulu, HI, USA, Jun. 2017, pp. 384-387.
- [35] A. Kord, D. L. Sounas, and A. Alù, "Low-Loss Broadband Magnetless Circulators for Full-Duplex Radios," in *Proc. IEEE MTT-S Int. Microw. Symp. (IMS)*, Philadelphia, PA, USA, Jun. 2018, pp. 506-509.
- [36] N. Reiskarimian and H. Krishnaswamy, "Magnetic-free non-reciprocity based on staggered commutation," *Nat. Commun.* **7**, 11217 (2016).
- [37] N. Reiskarimian, J. Zhou, and H. Krishnaswamy, "A CMOS Passive LPTV Non-Magnetic Circulator and Its Application in a Full-Duplex Receiver," *IEEE J. Solid-State Circuits* **52**, 1358 (2017).
- [38] T. Dinc, M. Tymchenko, A. Nagulu, D. Sounas, A. Alù, and H. Krishnaswamy, "Synchronized conductivity modulation to realize broadband lossless magnetic-free non-reciprocity," *Nat. Commun.* **8**, 795 (2017).
- [39] A. Nagulu, A. Alù, and H. Krishnaswamy, "Fully-Integrated Non-Magnetic 180nm SOI Circulator with $>1\text{W}$ P1dB, $>+50\text{dBm}$ IIP3 and High Isolation Across 1.85 VSWR," in *Proc. IEEE Radio Freq. Integ. Circuits Symp. (RFIC)*, Philadelphia, PA, USA, Jun. 2018, pp. 104-107.
- [40] M. M. Biedka, R. Zhu, Q. M. Xu, and Y. E. Wang, "Ultra-Wide Band Non-reciprocity through Sequentially-Switched Delay Lines," *Sci. Rep.* **7**, 40014 (2017).
- [41] M. M. Biedka, Q. Wu, X. Zou, S. Qin, and Y. E. Wang, "Integrated time-varying electromagnetic devices for ultra-wide band nonreciprocity," in *Proc. IEEE Radio Wireless Symp. (RWS)*, Anaheim, CA, USA, Jan. 2018, pp. 80-83.
- [42] S. Qin, Q. Xu, and Y. E. Wang, "Nonreciprocal components with distributedly modulated capacitors," *IEEE Trans. Microw. Theory Techn.* **62**, 2260 (2014).
- [43] M. M. Torunbalci, T. J. Odelberg, S. Sridaran, R. C. Ruby, and S. A. Bhave, "An FBAR Circulator," *IEEE Microw. Wireless Compon. Lett.* **28**, 395 (2018).

- [44] C. Xu, E. Calayir, and G. Piazza, “Magnetic-free electrical circulator based on AlN MEMS filters and CMOS RF switches,” in *Proc. 31st IEEE Int. Conf. Micro Electro-Mech. Sys. (MEMS)*, Belfast, UK, Jan. 2018, pp. 755-758.
- [45] Y. Yu, G. Michetti, A. Kord, D. Sounas, F. V. Pop, P. Kulik, M. Pirro, Z. Qian, A. Alù, “Magnetic-Free Radio Frequency Circulator based on Spatiotemporal Commutation of MEMS Resonators,” in *Proc. 31st IEEE Int. Conf. Micro Electro-Mech. Sys. (MEMS)*, Belfast, UK, Jan. 2018, pp. 154-157.
- [46] Y. Yu, F. Pop, G. Michetti, P. Kulik, M. Pirro, M. Rinadli, A. Kord, D. Sounas, A. Alù, “2.5 GHz Highly-Linear Magnetic-Free Microelectromechanical Resonant Circulator,” in *Proc. IEEE Int. Freq. Cont. Symp. (IFCS)*, Olympic Valley, CA, May 2018.
- [47] R. Fleury, D. L. Sounas, C. F. Sieck, M. R. Haberman, and A. Alù, “Sound isolation and giant linear nonreciprocity in a compact acoustic circulator,” *Science* **343**, 516 (2014).
- [48] Z. Yu and S. Fan, “Complete optical isolation created by indirect interband photonic transitions,” *Nat. Photon.* **3**, 91 (2009).
- [49] H. Lira, Z. Yu, S. Fan, and M. Lipson, “Electrically driven nonreciprocity induced by interband photonic transition on a silicon chip,” *Phys. Rev. Lett.* **109**, 033901 (2012).
- [50] K. Fang, Z. Yu, and S. Fan, “Photonic Aharonov–Bohm effect based on dynamic modulation,” *Phys. Rev. Lett.* **108**, 153901 (2012).
- [51] L. Fan, J. Wang, L. T. Varghese, H. Shen, B. Niu, Y. Xuan, A. M. Weiner, and M. Qi, “An all-silicon passive optical diode,” *Science* **335**, 447 (2012).
- [52] A. M. Mahmoud, A. R. Davoyan, and N. Engheta, “All-passive nonreciprocal metastructure,” *Nat. Commun.* **6**, 8359 (2015).